Supporting Information

Tailoring C-F Configurations in O-CF_x Cathodes *via* Wet Chemistry for 600 Wh kg^{-1} Li/O-CF_x Pouch Cells

Zhenghuai Sun[1,#], Xiaobin Liao[4,#], Luyu Li[1,#], Quan Yuan[1], Bingbing Chen[5], Chunbo Xu[5], Hancheng Ma[6], Huji Zhang[7], Xiangning Chen[1], Zihan Liu[1], Xu Xu[1], Yao Ding[1,2,], Ruizhe Wu[3,*], Liqiang Mai[1,*]*

[1]State Key Laboratory of Advanced Technology for Materials Synthesis and Processing, Wuhan, P.R. China.

[2]Hubei Longzhong Laboratory, Xiangyang, P.R. China.

[3]Collaborative Innovation Center for Advanced Organic Chemical Materials Co-constructed by the Province and Ministry, Ministry of Education Key Laboratory for the Synthesis and Application of Organic Functional Molecules, College of Chemistry and Chemical Engineering, Hubei University, Wuhan, P.R. China.

[4]School of Marine Technology and Equipment, Hainan University, Haikou, P.R. China.

[5]Wuhan Institute of Marine Electric Propulsion, Wuhan, P.R. China.

[6]Department of Chemical and Biological Engineering and William Mong Institute of Nano Science and Technology, Hong Kong University of Science and Technology, Clear Water Bay, Kowloon, Hong Kong, P.R. China.

[7]Hubei Huitian New Materials Co., Ltd., National High-tech Industrial Development Zone, No. 1, Guanyu Road, Xiangyang, P. R. China.

[#]Z. Sun, X. Liao and L. Li contributed equally to this work.

[*] Corresponding authors.

E-mail addresses: ydingaf@whut.edu.cn (Y. Ding), wuruizhe@hubu.edu.cn (R. Wu), mlq518@whut.edu.cn (L. Mai)

Keywords: CF_x, Oxidation, C-F configurations, Primary lithium battery, High-rate capability

1. Experimental Section

1.1 Materials

All CF_x materials were purchased from Shandong Chongshan Optoelectronic Materials Co. LTD. The commercial electrolyte was purchased from Jiangxi Hairong New Materials Co. LTD., model HR-6002. Concentrated sulfuric acid and concentrated nitric acid were purchased from Sinopharm Group Chemical Reagent Co.LTD. Lithium perchlorate, 1, 3-dioxopentane (DOL), propylene carbonate (PC) and methyl propionate (MP) were purchased from Duoduo Chemical Reagent Network.

1.2 Acid treatment of CF_x (O-CF_x)

Synthesis of O-CFx-2: 1 g CF_x (x = 0.6, Shandong Zhongshan Photoelectric Materials Co., Ltd.) were mixed with 75 mL of concentrated H_2SO_4 and 25 mL of concentrated HNO_3. After 1 h ultrasonication, Condensation and reflux at different temperatures (80~120 ℃) for 6~12 h with constant stirring during the reflux process. After reaction, oxidized CF_x (O-CF_x) was filtered through a microporous membrane and washed with deionized (DI) water until the pH = 7. Finally, the oxidized product was obtained by vacuum drying at 80 °C for 12 h. The synthesis methods of the comparison samples were the same. The acidification temperature and time are shown in Table S1.

1.3 Electrochemical measurements

Coin cells (CR2025-type) assembled in an argon-filled glove box. Mix 80 wt.% of the active material (CF_x, O-CF_x-1, O-CF_x-2, O-CF_x-3, O-CF_x-4, O-CF_x-5), Super P (10 wt.%) and PVDF (10 wt.%) together to make the cathode, then add NMP to the uniformly mixed powder to make the slurry, and finally coating it on the aluminum foil (the thickness of the scraper used for coating is 50-100 μm). Cut into raw sheets with a diameter of 10 mm. The electrolyte was prepared by directly dissolving 1.0 M $LiClO_4$ in a mixture of DOL:PC:MP=1:1:12 (v/v/v). Using raw sheets as the positive electrode, lithium foil as the negative electrode, and polypropylene (PP) as the separator. The button cell is mainly composed of the negative electrode shell, negative electrode lithium sheet, separator, electrolyte, electrode sheet, gasket, spring sheet and positive electrode shell. The amount of electrolyte in each coin battery is approximately 70 μL.

All cells were allowed to stand to ensure adequate electrolyte penetration. In this study, the LAND-2001A electrochemical channel was used to test the discharge specific capacity, rate performance, specific power, specific energy of lithium/fluorocarbon batteries, and to analyze the relative magnitude of the Li^+ chemical diffusion coefficient. The electrochemical impedance spectra were tested using the AutolabPGSTAT302N electrochemical workstation.

1.4 Material characterizations

X-ray diffraction (XRD) measurement was performed using a Bruker AXS D2 Advance powder X-ray diffractometer with a detector using Cu Kα X-ray source. Raman characterizations were measured with green laser (532 nm) using LABRAM HR Evolution Raman spectrometer. X-ray photoelectron spectroscopy (XPS) was performed using a VG MultiLab 2000 instrument. Aberration-corrected high-angle annular dark field scanning transmission electron microscopy (HAADF-STEM), transmission electron microscopy (TEM), and high-resolution transmission electron microscopy (HRTEM) images were acquired using a Titan G2 60-300 with an energy-dispersive X-ray (EDX) spectrometer. The distribution of elements was analyzed by using the Nano TOF III time-of-flight secondary ion mass spectrometer released by Ulvac-Phi Corporation of Japan.

1.5 Assembling of coin cells and 21 Ah Li/O-CF_x pouch cells

Coin cells: For the assembling of coin-cells, the cathode disc has a diameter of 10 mm (area ≈ 0.785 cm^2) with an active-material loading of ~2.6 mg (≈ 3.27 mg cm^{-2}). The electrolyte amount is ~70 μL per cell, corresponding to an E/C ratio of ≈ 70 μL mg^{-1} (≈ 89 μL cm^{-2}). The rate/polarization comparisons among different samples were performed under the consistent electrode-level design parameters with sufficiently excess electrolyte.

21 Ah pouch cells: the O-CF_x cathode (91 wt.% of O-CF_x, 5 wt.% of Super P and 4 wt.% of PVDF) was coated on both sides of a 10 μm-thick aluminum foil, with a double-sided areal density of 24 mg/cm^2 and a compacted density of 1.3 g/cm^3. The anode was a 90 μm-thick pure Li strip (supplied by Nantong Shengneng Advanced

Materials Technology Co., Ltd.), which was bonded to a 6 μm-thick Cu foil serving as the current collector. The separator consisting of a 9 μm-thick polyethylene layer and a 3 μm-thick Al_2O_3 layer was applied. The 21 Ah pouch cell was assembled by stacking 21 cathode sheets and 22 anode sheets alternately.

1.6 DFT calculations

All spin-polarized density functional theory (DFT) calculations were conducted using the Vienna Ab initio Simulation Package (VASP). The generalized gradient approximation (GGA) with the Pedew-Burke-Ernzerhof (PBE) functional was employed to describe the electron exchange-correlation interactions. A plane-wave cutoff energy of 520 eV was set to ensure convergence, with energy and force convergence criteria defined as 1.0×10^{-5} eV per atom and 0.02 eV/ A respectively. Structural relaxations were performed using the conjugate gradient (CG) algorithm until these criteria were satisfied. The GAMMA scheme with a 1×1×1 k-point mesh was used for Brillouin zone sampling to balance computational efficiency and accuracy.

The weak van der Waals interactions and long-range corrections between adsorbates and the substrate were incorporated via the DFT-D3 method with BJ damping, ensuring proper description of non-covalent interactions in the system.

1.7 Gaussian calculations

The binding energies and ESP population of the molecules were calculated by the Gaussian software. The m062x functional with the def2tzvp basis set and DFT-D3 dispersion were selected for the geometry optimization and single-point energy.

1.8 MD calculations

Molecular dynamic (MD) simulations of three electrolytes are performed using the Forcite module in the Materials Studio software. All the MD simulations employed a condensed-phase optimized molecular potentials for atomistic simulation studies (COMPASS III) force field. The temperature was set to be 300 K with the Andersen thermostat. The time step is fixed to be 1 fs for the NVT equilibrium. The canonical ensemble (NVT) at 300 K with total time of 5 ns is further carried out for the production runs and for statistical analysis. Note that long simulation time is necessary for ensuring

the equilibrium states of the electrolytes systems.

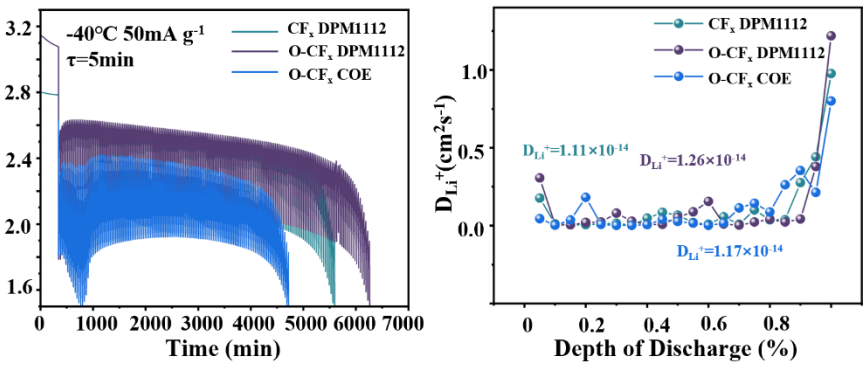

Figure S1. Galvanostatic intermittent titration technique (GITT) and Li^+ diffusion coefficient (D_{Li}^+) for CF_x and O-CF_x cathodes with COE and DPM-1112.

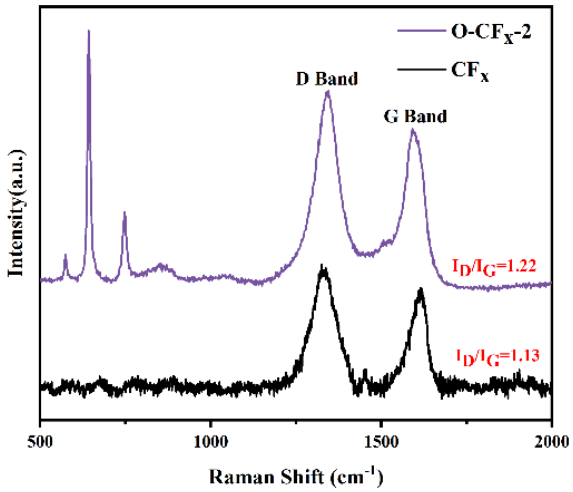

Figure S2. Raman spectrum before discharge of CF_x and O-CF_x-2 and the intensity ratio of D/G bands (I_D/I_G)

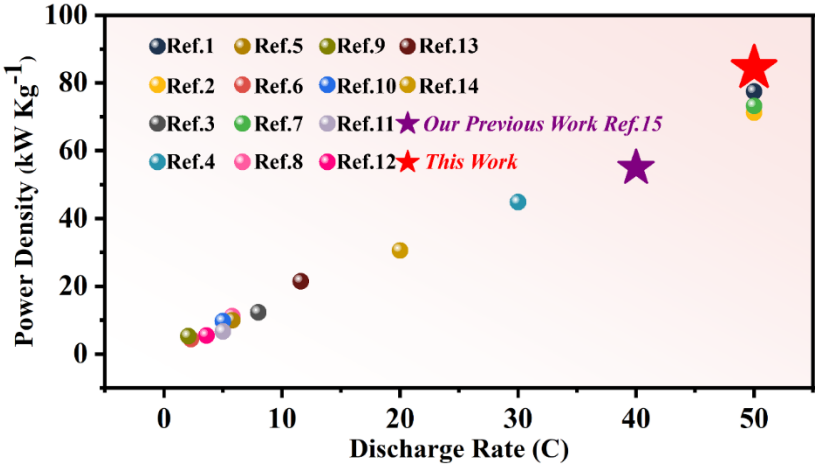

Figure S3. Discharge rates and power density of O-CF_x-2 compared with previously reported CF_x cathodes.

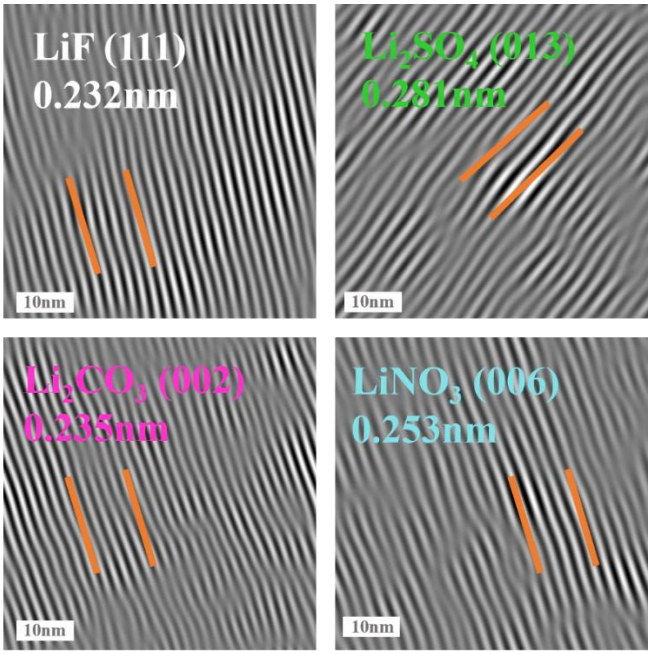

Figure S4. TEM images of additional discharge products of O-CF_x-2 cathodes with DPM.

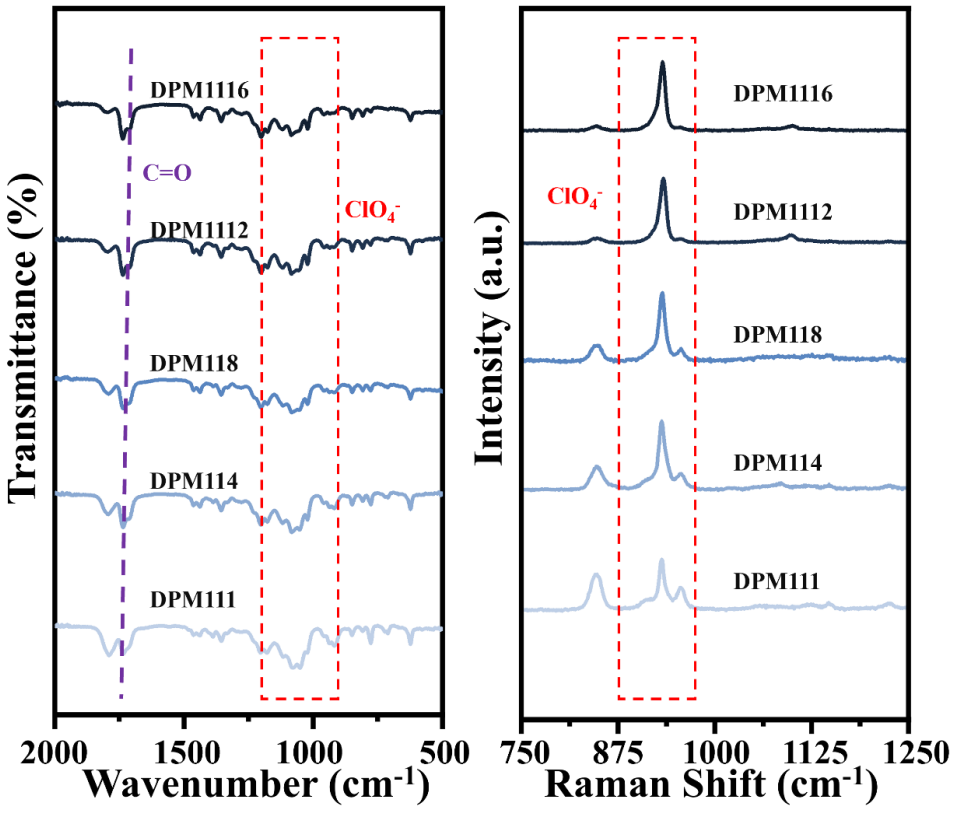

Figure S5. FT-IR and Raman spectra of DPM with different concentration of MP.

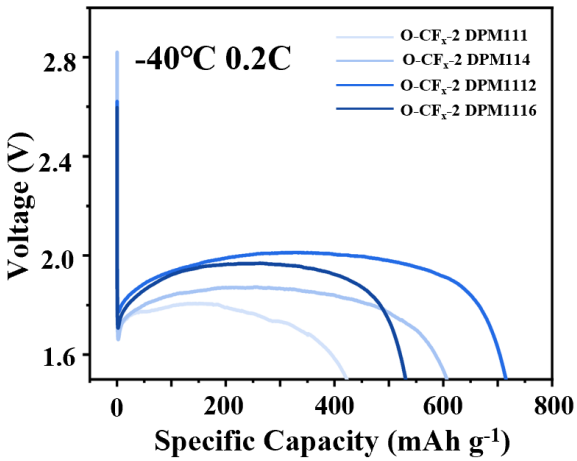

Figure S6. Electrochemical performance of DPM with different concentration of MP.

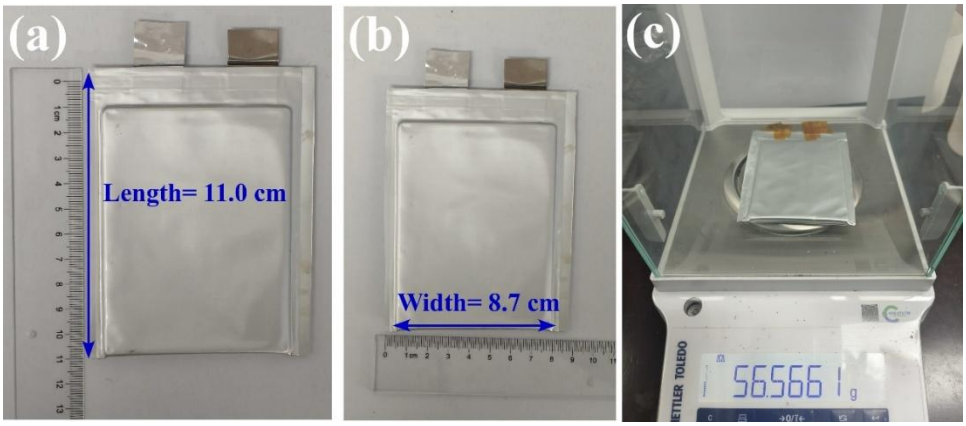

Figure S7. (a) and **(b)** Length (a) and width (b) of the 21 Ah Li/O-CF_x pouch cell. **(c)** Weight of the 21 Ah Li/O-CF_x pouch cell before discharge.

Figure S8. Applications of a single 21 Ah Li/O-CF_x pouch cell on an unmanned aerial vehicle.

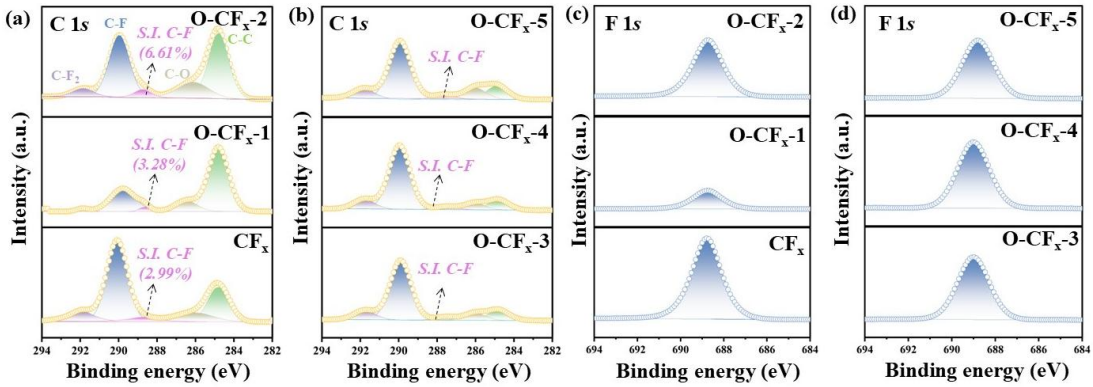

Figure S9. (a-b) XPS C1*s* spectra of pristine CF_x and O-CF_x at different oxidation conditions. (c-d) XPS F1*s* spectra of pristine CF_x and O-CF_x at different oxidation conditions.

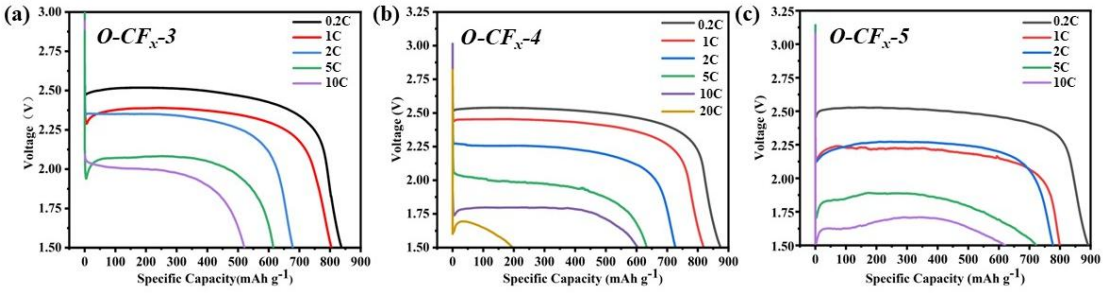

Figure S10. Electrochemical performance of O-CF_x-3 (a), O-CF_x-4 (b) and O-CF_x-5 (c).

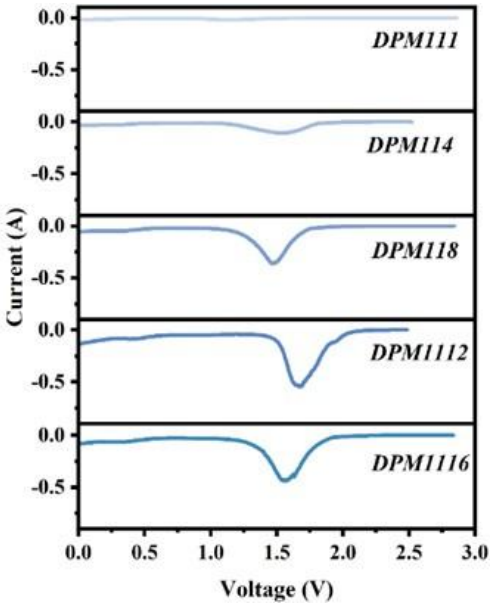

Figure S11. The linear sweep voltammetry (LSV) tests for different ratios of DPM electrolyte.

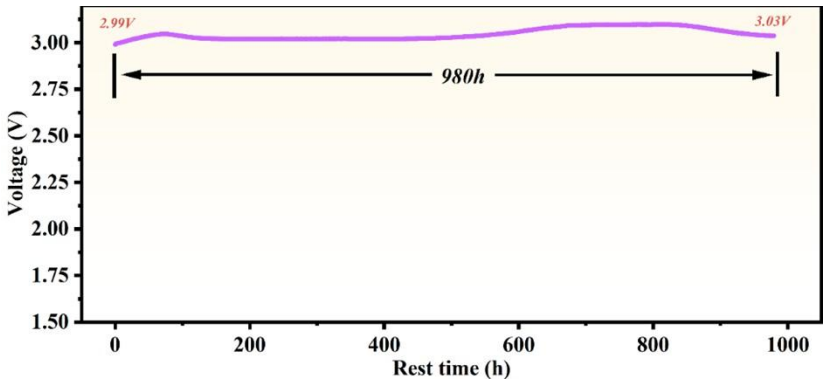

Figure S12. The voltage variation of Li/O-CF_x batteries during rest time.

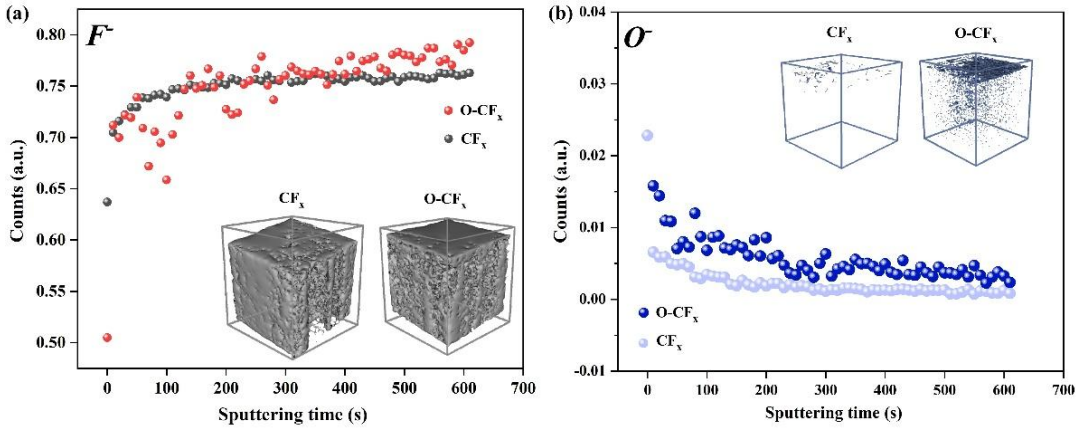

Figure S13. Depth-resolved ToF-SIMS and the corresponded 3D plot of F^- (a) and O^- (b) in CF_x and O-CF_x.

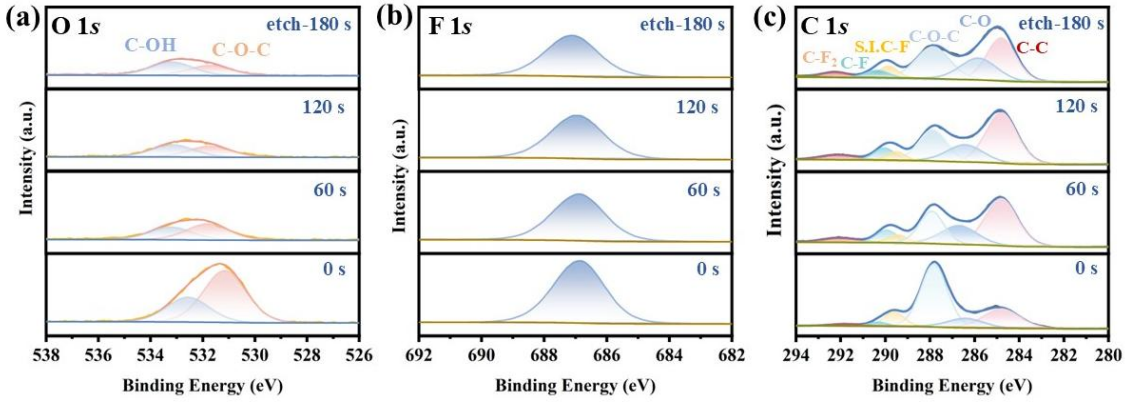

Figure S14. XPS depth profiling analysis of O-CF_x for F 1*s* (a), O 1*s* (b) and C 1s (c) spectra.

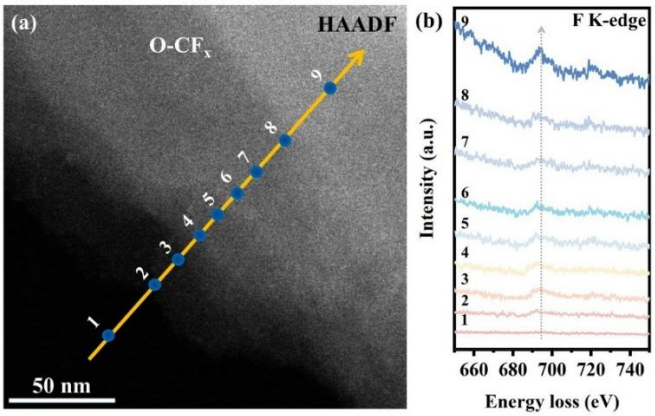

Figure S15. TEM-HAADF image of O-CF$_x$ (a) and the corresponded EELS analysis of F K-edge linear plot with the increase of thickness (b).

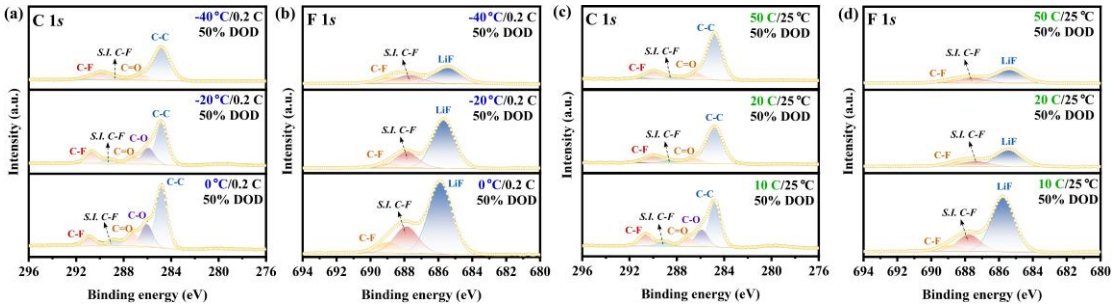

Figure S16. The C 1*s* (a) and F 1*s* (b) XPS spectra of O-CF$_x$-2 cathode discharged at 0 to -40 °C, 0.2 C and 50% DoD. The C 1*s* (c) and F 1*s* (d) XPS spectra of O-CF$_x$-2 cathode discharged at 10 to 50 C, 25 °C and 50% DoD.

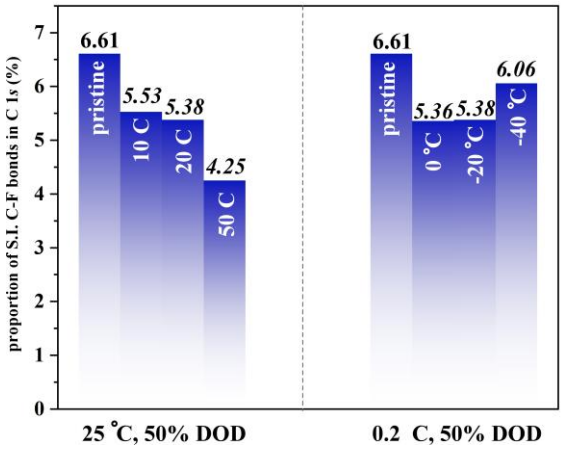

Figure S17. Proportion of the semi-ionic C-F bonds at 50% depth of discharge (DOD) under different conditions (based on integrated peak area).

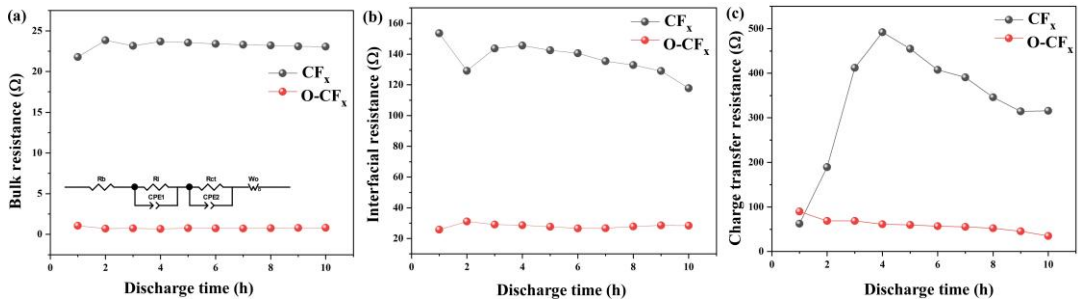

Figure S18. Bulk resistance (a), interfacial resistance (b) and charge transfer resistance (c) of Li/CF_x and Li/O-CF_x batteries with COE electrolyte at room temperature.

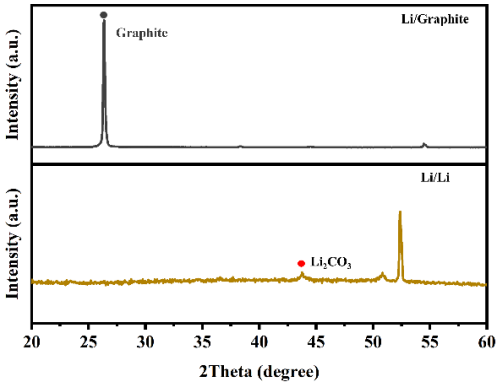

Figure S19. XRD patterns of the cathodes from discharged Li||Li symmetric cells and Li||Graphite cells with DPM1112.

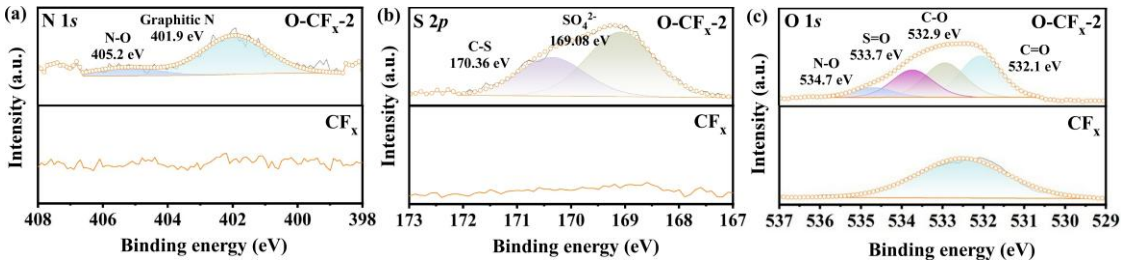

Figure S20. N 1*s* (a), S 2*p* (b) and O 1*s* (c) XPS spectra of O-CF_x-2 and CF_x.

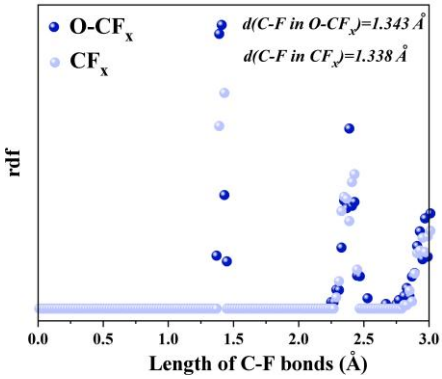

Figure S21. Radial distribution function (RDF) analysis of C-F bonds in CF_x and O-CF_x models.

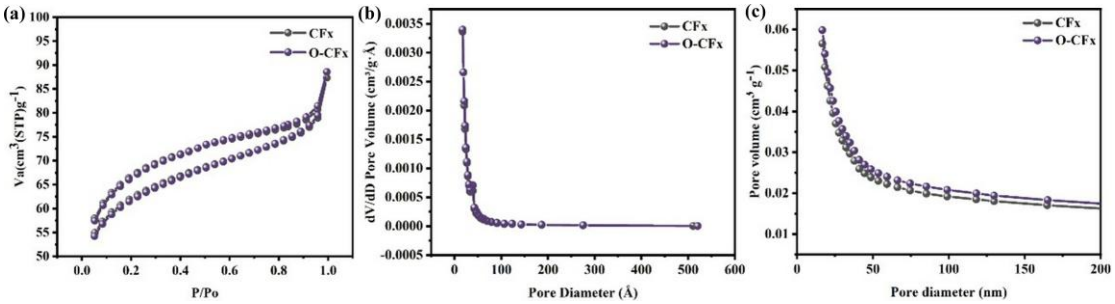

Figure S22. (a) N_2 adsorption-desorption isotherms, (b) pore-size distributions and (c) pore-volume vs. pore-diameter plots of CF_x and O-CF_x.

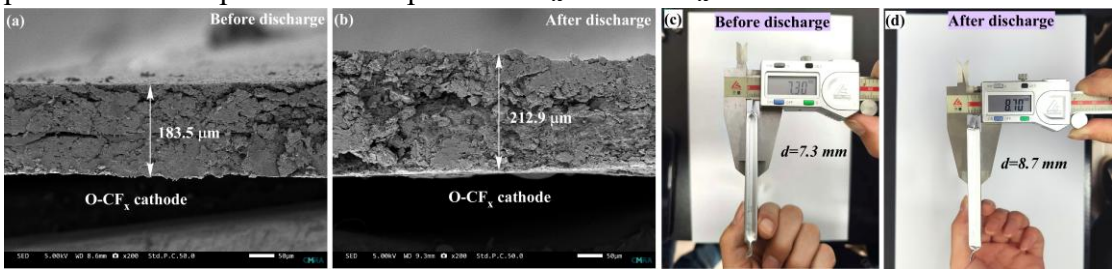

Figure S23. Cross-sectional morphology for a single cathode in the 21 Ah Li/O-CF_x pouch cells by SEM characterizations before (a) and after (b) discharge. Digital microscopy of the 21 Ah Li/O-CF_x pouch cells before (c) and after (d) discharge.

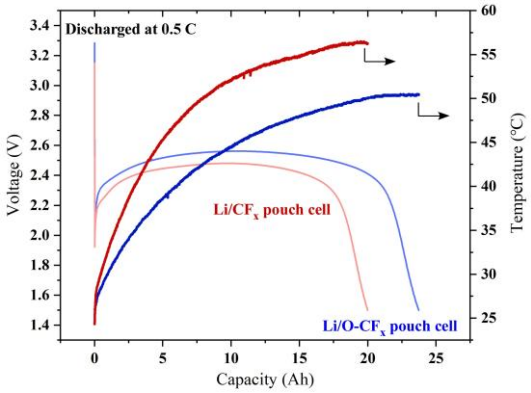

Figure S24. Capacity and temperature profiles of Li/CF_x and Li/O-CF_x pouch cells discharge at 25 °C.

Table S1. Different treatment time and temperature of O-CF_x-1, O-CF_x-2, O-CF_x-3, O-CF_x-4 and O-CF_x-5.

Sample	Oxidation Time (h)	Oxidation Temperature (℃)
O-CF_x-1	6	100
O-CF_x-2	12	100
O-CF_x-3	6	80
O-CF_x-4	12	80
O-CF_x-5	16	100

Table S2. The oxygen content, fluorine content and F/C of different acidified pre-treated fluorocarbon materials.

Reaction conditions for acidification treatment	O/At.%	F/At.%	F/C ratio
0 ℃&0 h（CF_x）	5.96	43.08	0.62
100 ℃&6 h（O-CF_x-1）	11.01	33.13	0.47
100 ℃&12 h（O-CF_x-2）	13.12	40.64	0.52

Table S3. Comparison of the low temperature electrochemical performance between O-CF_x materials in DPM1112, and other research studies.

No.	Electrolyte	Tempertature (°C)	Discharge current density or rate	Cutoff voltage (V)	Capacity (mAh/g)	Reference
1	1 M $LiClO_4$ in TTE:DME:PC (2:2:1, v/v/v)	-50	100 mA/g	1.5	300	(**ACS Applied Energy Materials** 2021, 4 (4), 3777–3784)[16]
2	1 M $LiBF_4$ in DME:PC (1:1 v/v)	-50	80 mA/g	1	74	(**Energy Storage Materials** 2022, 50, 598–605)[17]
3	0.8 M $LiBF_4$ -0.2 M LiFSI/ PC:DME:Isobutyle acetate	-60			445	
4	0.5M $LiBF_4$ in AN:GBL (1:1 w/w)	-50	0.02 C	1.5	～565	（**Journal of Power Sources** 2009，188，532-537) [18]
5	0.5M LiBF4 in PC:DME (1:1 w/w)				～320	
6	1M LiFSI in PC:Methyl-Butyrate (1:2 v/v)	-40	80 mA/g	0.5	813	(**Energy Storage Materials** 2021, 42, 477–483.)[19]
7	1M $LiBF_4$ in EC:MA (1:9 w/w)+1.00 wt.% Sn(OTf)2	-40	100 mA/g	1.5	788	(**Advanced Functional Materials** 2025, 35 (3), 2413423)[20]
8	1 M LiBF4 in Me_2O-PC	-60	10 mA/g	1.5	780	(**Advanced Materials** 2023, 35 (3),
9		-70			603	

	(1:1 v/v)					2207932)[21]
10	1M $LiBF_4$ in γ-butyrolactone with 2 vol% 15-crown-5 additive	-40	6.67 mA/g	0.5	50	**(Journal of The Electrochemical Society** 2017，164（13），A3109-A3116)[22]
11	1M $LiBF_4$ in PC:TFPC:DME (15:5:80 v/v/v)	-40	0.1 C	0.5	20	**(Electrochemical and Solid-state Letters** 10（7）A166-A170 2007)[23]
12	1M $LiBF_4$ in DME:PC (2:8 v/v)+1.5% VC	-40			10	
13	0.5 M $LiBF_4$ in DME:PC (2:8 v/v)	-40			695	
This work	1 M $LiClO_4$ in PC:DOL:MP (1:1:12)	-40	0.2 C	1.5	716	***This Work***
This work			0.5 C		466	

Table S4. Comparison of reported energy densities of lithium pouch cells at different temperatures with this work.

Temperature (°C)	Specific energy density (Wh kg^{-1})	Current density (mA g^{-1})	Pouch cells	Reference
30	**642.08**	**173**	**15 Ah Li||O-CF_x**	***This work***
	628.55	**432.5**		
	554.99	**865**		
-40	**324.09**	**173**		
	181.17	**432.5**		
-60	126	120	0.16 Ah Li|| SPAN	*Nat. Energy (2021)* [24]
-40	143			
23	218			
-85	171.8	20	0.5 Ah Li || NMC811	*Nat. Commun. (2025)* [25]
-50	150	200		
-40	175	198	0.5 Ah Li || NMC811	*Energy Environ. Sci. (2024)* [26]
-60	301	198		
-85	122	19.3		
23	307	40	5 Ah Li || NMC811	*Energy Environ. Sci. (2022)* [27]
-20	250			
-40	230			
25	403	~20	2.7 Ah Li || NMC811	*Adv. Energy Mater. (2025)* [28]
-20	320			
-40	200			

-50	159	~10		
25	426	~214	0.32 Ah Li || NMC811	*Nat. Commun. (2023)* [29]
0	~350			
-20	~300			
-30	~270			
-60	~160			
25	450	~20	2.9 Ah Li || NMC811	*Energy Environ. Sci. (2025)* [30]
-20	350			
-40	270	~10	2 Ah Gr || NMC523	*Adv. Mater. (2023)* [31]
-60	50	261	7 Ah MCMB carbon || $LiNiCoO_2$	*J. Electrochem. Soc (2010)* [32]
-50	70			
-40	82			
-30	90			
-20	100			
28	459.05	865	5.5 Ah Li || CF_x	*Energy Environ. Sci. (2025)* [33]
-20	233			
-40	168			

References

[1] Z. Luo, X. Wang, D. Chen, Q. Chang, S. Xie, Z. Ma, W. Lei, J. Pan, Y. Pan, J. Huang, *ACS Applied Materials & Interfaces* **2021**, 13, 18809-18820.

[2] J. Ma, Y. Liu, Y. Peng, X. Yang, J. Hou, C. Liu, Z. Fang, X. Jian, *Composites Part B: Engineering* **2022**, 230, 109494.

[3] Y. Peng, Y. Liu, R. Ali, J. Ma, J. Hou, X. Yang, X. J *Journal of Alloys and Compounds* **2022**, 905, 164151.

[4] Y. Dai, S. Cai, L. Wu, W. Yang, J. Xie, W. Wen, J.-C. Zheng, Y. Zhu, *Journal of Materials Chemistry A* **2014**, 2, 20896-20901.

[5] J. Ban, X. Jiao, Y. Feng, J. Xue, C. He, J. Song, *ACS Applied Energy Materials* **2021**, 4, 3777-3784.

[6] C. Zhu, X. Shen, Z. Gao, Y. Li, X. Wu, J. Zhao, P. Zhou, S. Zhuo, J. Zhou, *Electrochimica Acta* **2022**, 425,140718.

[7] L. Kong, Y. Li, C. Peng, L. Sun, K. Wang, Y. Liu, W. Feng, *Nano Energy* **2022**, 104, 107905.

[8] L. Sun, C. Peng, L. Kong, Y. Li, W. Feng, *Energy & Environmental Materials* 2022, 6, e12323.

[9] Q. Li, W. Xue, X. Sun, X. Yu, H. Li, L. Chen, *Energy Storage Materials* **2021**, 38, 482-488.

[10] Y. Zhu, L. Zhang, H. Zhao, Y. Fu, *Journal of Materials Chemistry A* **2017**, 5, 796-803.

[11] Y. Li, W. Feng, *Journal of Power Sources* **2015**, 274, 1292-1299.

[12] L. Wang, Y. Li, S. Wang, P. Zhou, Z. Zhao, X. Li, J. Zhou, S. Zhuo, *ChemElectroChem* **2019**, 6, 2201-2207.

[13] G. Zhong, H. Chen, X. Huang, H. Yue, C. Lu, *Frontiers in Chemistry* **2018**, 6, 50.

[14] K. Wang, Y. Feng, L. Kong, C. Peng, Y. Hu, W. Li, Y. Li, W. Feng, *Energy & Environmental Materials* **2022**, 0,e12437.

[15] L. Li, R. Wu, H. Ma, B. Cheng, S. Rao, S. Lin, C. Xu, L. Li, Y. Ding, L. Mai, *Small* **2023**, e2300762.

[16] J. Ban, X. Jiao, Y. Feng, J. Xue, C. He, J. Song, *ACS Applied Energy Materials* **2021**, 4, 3777-3784.

[17] W. Xue, T. Qin, Q. Li, M. Zan, X. Yu, H. Li, *Energy Storage Materials* **2022**, 50, 598-605.

[18] S. S. Zhang, D. Foster, J. Read, *Journal of Power Sources* **2009**, 188, 532-537.

[19] Z. Fang, Y. Yang, T. Zheng, N. Wang, C. Wang, X. Dong, Y. Wang, Y. Xia, *Energy Storage Materials* **2021**, 42, 477-483.

[20] X. Chen, G. Liu, A. Fu, Y. Xiao, J. Sun, Z. Zhang, Y. Yang, *Advanced Functional Materials* **2025**, 35, 2413423.

[21] Y. Yin, J. Holoubek, A. Liu, B. Sayahpour, G. Raghavendran, G. Cai, B. Han, M. Mayer, N. B. Schorr, T. N. Lambert, K. L. Harrison, W. Li, Z. Chen, Y. S. Meng, *Advanced Materials* **2023,** 35, e2207932.

[22] J.-P. Jones, S. C. Jones, F. C. Krause, J. Pasalic, M. C. Smart, R. V. Bugga, E. J. Brandon, W. C. West, *Journal of The Electrochemical Society* **2017**, 164, A3109.

[23] J. Whitacre, W. West, M. Smart, R. Yazami, S. Prakash, A. Hamwi, B. V. Ratnakumar, *Electrochemical and Solid State Letters* **2007**, 10.

[24] J. Holoubek, H. Liu, Z. Wu, Y. Yin, X. Xing, G. Cai, S. Yu, H. Zhou, T. A. Pascal, Z. Chen, P. Liu, *Nature Energy* **2021**, 6, 303-313.

[25] W. Zhang, Y. Lu, Q. Feng, H. Wang, G. Cheng, H. Liu, Q. Cao, Z. Luo, P. Zhou, Y. Xia, W. Hou, K. Zhao, C. Du, K. Liu, *Nature Communications* **2025**, 16, 3344.

[26] W. Zhang, Y. Lu, Q. Cao, H. Liu, Q. Feng, P. Zhou, Y. Xia, W. Hou, S. Yan, K. Liu, *Energy & Environmental Science* **2024**, 17, 4531-4543.

[27] J. Holoubek, K. Kim, Y. Yin, Z. Wu, H. Liu, M. Li, A. Chen, H. Gao, G. Cai, T. A. Pascal, P. Liu, Z. Chen, *Energy & Environmental Science* **2022**, 15, 1647-1658.

[28] Z. Li, Y. Liao, H. Ji, X. Lin, Y. Wei, S. Hao, X. Hu, L. Yuan, Z. Huang, Y. Huang, *Advanced Energy Materials* **2025**, 15, 2404120.

[29] G. Zhang, J. Chang, L. Wang, J. Li, C. Wang, R. Wang, G. Shi, K. Yu, W. Huang, H. Zheng, T. Wu, Y. Deng, J. Lu, *Nature Communications* **2023**, 14, 1081.

[30] Y. Wei, H. Wang, X. Lin, T. Wang, Y. Cui, Y. Huang, J. Yang, T. Liu, Y. Ren, X.

Fan, H. Xu, Y. Huang, *Energy & Environmental Science* **2025**, 18, 786-798.

[31] X. Zheng, Z. Cao, W. Luo, S. Weng, X. Zhang, D. Wang, Z. Zhu, H. Du, X. Wang, L. Qie, H. Zheng, Y. Huang, *Advanced Materials* **2023**, 35, 2210115.

[32] M. C. Smart, B. V. Ratnakumar, K. B. Chin, L. D. Whitcanack, *Journal of the Electrochemical Society* **2010**, 157, A1361-A1374.

[33]J. Huang, S. Zhang, B. Wan, W. Liu, R. Li, Z. Yang, L. Li, J. Hua, F. Chu, M. Li, T. Zhou, J. Wang, Y. Wu, Z. Li, L. Fan, L. Chen, T. Deng, X. Fan, *Energy & Environmental Science* **2025**, 18, 10328-10337.